Neuron

Time and experience differentially affect distinct aspects of hippocampal representational drift

Graphical abstract

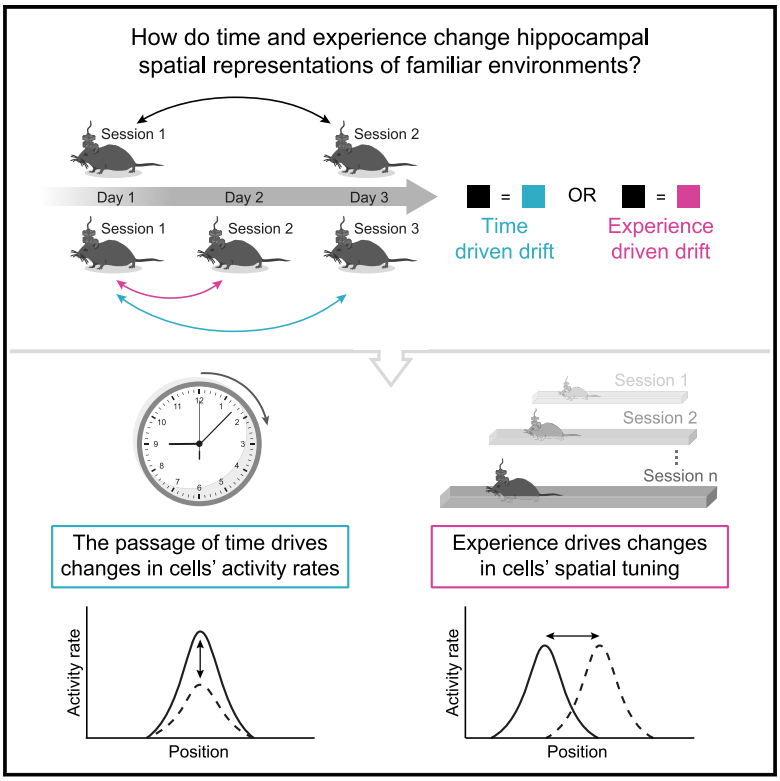

Highlights

- Hippocampal neurons exhibit representational drift in familiar environments over weeks
- The passage of time drives changes in neuronal activity rates
- Experience drives changes in neuronal spatial tuning
- Drift in a given environment is unaffected by experience in another environment

Authors

Nitzan Geva, Daniel Deitch, Alon Rubin, Yaniv Ziv

Correspondence

alon.rubin@weizmann.ac.il (A.R.), yaniv.ziv@weizmann.ac.il (Y.Z.)

In brief

Geva et al. find a double dissociation between the effects of time and experience on distinct aspects of hippocampal representational drift (i.e., the gradual change in neuronal representations of familiar environments): the passage of time drives changes in neuronal activity rates, whereas experience drives changes in the cells' spatial tuning.

Geva et al., 2023, Neuron *111*, 1–10
August 2, 2023
https://doi.org/10.1016/j.neuron.2023.05.005

CellPress

Please cite this article in press as: Geva et al., Time and experience differentially affect distinct aspects of hippocampal representational drift, Neuron (2023), https://doi.org/10.1016/j.neuron.2023.05.005

Neuron

CellPress

Report

Time and experience differentially affect distinct aspects of hippocampal representational drift

Nitzan Geva,[1,2] Daniel Deitch,[1,2] Alon Rubin,[1,3,*] and Yaniv Ziv[1,3,4,*]
[1]Department of Brain Sciences, Weizmann Institute of Science, Rehovot, Israel
[2]These authors contributed equally
[3]These authors contributed equally
[4]Lead contact
*Correspondence: alon.rubin@weizmann.ac.il (A.R.), yaniv.ziv@weizmann.ac.il (Y.Z.)
https://doi.org/10.1016/j.neuron.2023.05.005

SUMMARY

Hippocampal activity is critical for spatial memory. Within a fixed, familiar environment, hippocampal codes gradually change over timescales of days to weeks—a phenomenon known as representational drift. The passage of time and the amount of experience are two factors that profoundly affect memory. However, thus far, it has remained unclear to what extent these factors drive hippocampal representational drift. Here, we longitudinally recorded large populations of hippocampal neurons in mice while they repeatedly explored two different familiar environments that they visited at different time intervals over weeks. We found that time and experience differentially affected distinct aspects of representational drift: the passage of time drove changes in neuronal activity rates, whereas experience drove changes in the cells' spatial tuning. Changes in spatial tuning were context specific and largely independent of changes in activity rates. Thus, our results suggest that representational drift is a multi-faceted process governed by distinct neuronal mechanisms.

INTRODUCTION

Within a fixed, familiar environment, hippocampal codes gradually change over timescales ranging from minutes to weeks.[1–5] This phenomenon, termed representational drift,[6–8] has also been found in other brain areas, including the posterior parietal cortex[9] and sensory areas such as the visual cortex,[10,11] auditory cortex,[12] somatosensory cortex,[13] and piriform cortex.[14]

A common practice in longitudinal studies of hippocampal codes is to record the activity of the same neuronal population in a familiar environment that the animal repeatedly visits over days and weeks at fixed intervals.[3,4,15–18] Although this practice has proven itself useful for characterizing many of the properties of representational drift, it cannot be used to dissociate between the effects of the absolute passage of time and the amount of experience within the environment on the code's stability and long-term dynamics (Figure 1A). Thus, it has remained unclear how and to what extent time and experience drive changes in the neural code. This distinction is key to understanding the phenomenon of representational drift because time- and experience-dependent changes could point to different underlying biological mechanisms.

To tease apart the contribution of these two factors to representational drift, we used a within-subject design and longitudinally recorded the activity from the same hippocampal neurons in mice while they repeatedly explored two familiar environments,[4] which were visited at different intervals—one environment was visited every 2 days and the other every 4 days. If representational drift is exclusively time-dependent, the neuronal code for the two environments is expected to display the same level of similarity between visits that are separated by the same time interval (Figure 1B, top left) but to exhibit different levels of code similarity between visits separated by the same amount of experience (Figure 1B, top right). Alternatively, if the drift is exclusively experience-dependent, the similarity between representations should be the same in both environments for pairs of visits separated by the same amount of experience (Figure 1B, bottom right) but different across visits with the same time interval between them (Figure 1B, bottom left).

We found that the passage of time and the amount of experience differentially affected distinct aspects of hippocampal code stability: the passage of time was a more dominant factor than experience in driving changes in activity rates, whereas the amount of experience was more dominant than time in driving changes in the cells' spatial tuning.

RESULTS

We used head-mounted miniature fluorescence microscopes[3] to longitudinally record the activity of cells in the dorsal hippocampus CA1 in mice (n = 8) that repeatedly visited two different familiar linear-track environments at different time intervals over weeks (Figures 2A and 2B). The mice visited one of the

Please cite this article in press as: Geva et al., Time and experience differentially affect distinct aspects of hippocampal representational drift, Neuron (2023), https://doi.org/10.1016/j.neuron.2023.05.005

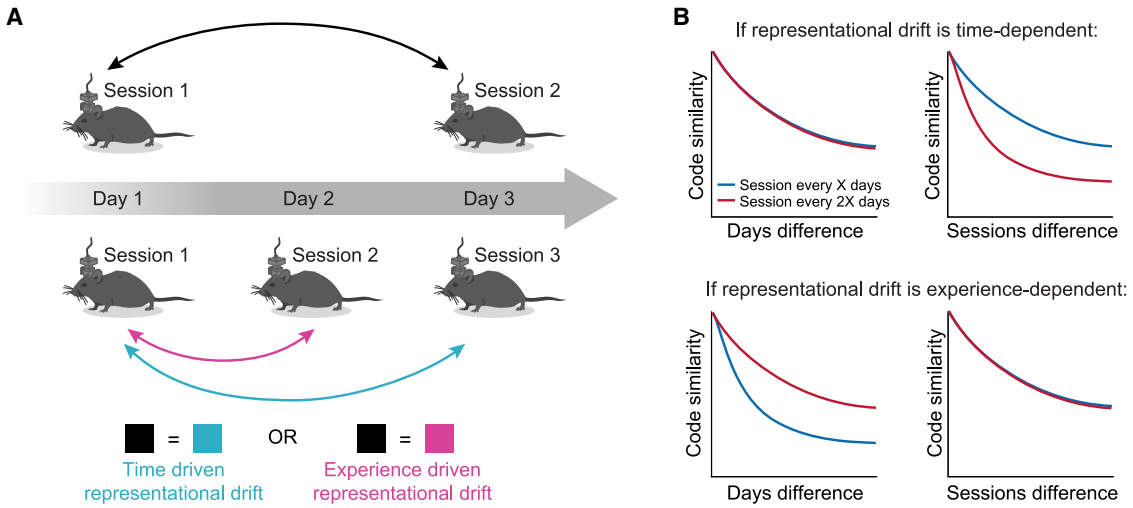

Figure 1. Elucidating the effects of time and experience on hippocampal representational drift

(A) Altering the time interval between recording sessions allows the dissociation between the effects of time and experience on representational drift.

(B) Possible outcomes. If representational drift is time-dependent, changes in neuronal activity patterns would be similar across pairs of visits with the same amount of time between them, irrespective of the amount of experience between them (top row). If representational drift is experience-dependent, changes in neuronal activity patterns would be similar across pairs of visits with the same amount of experience between them, irrespective of the amount of time between them (bottom row).

environments every 2 days (environment A) and the other every 4 days (environment B). This experimental design enabled us to dissociate between the effects of the passage of time and the amount of experience on the changes in the hippocampal activity patterns across sessions in each of the environments. We tracked the same neurons across multiple recording sessions throughout the experiment (666–1,109 cells per mouse, Figure 2C).[19] In all days of the experiment, place cells contributed to a population spatial representation that was reliable and unique for each location within the linear tracks (Figure 2D) while maintaining stable properties of neural code quality across days and environments (Figures S1A–S1G). The spatial representations of the two linear tracks were highly dissimilar (Figure 2E),[20,21] and this dissimilarity was also stable throughout the experiment (Figure S1H). Consistent with previous findings,[4] despite these stable facets of place cells' activity, spatial representations of the two environments exhibited gradual drift over days (Figures 2F and S2A).

To quantify hippocampal representational drift, we measured the similarity between the activity patterns across sessions in each of the two environments as a function of the time interval or as a function of the amount of experience (i.e., number of sessions) between two given sessions (Figures 1A and 1B).

We used complementary measures of neural code similarity to test the contribution of time and experience to two distinct aspects of representational drift (Figure 3A): (1) ensemble rate correlation, which captures the changes in the overall activity levels of individual neurons across sessions, and (2) tuning curve correlation, which captures the changes in the cells' spatial tuning. By calculating these measures across all pairs of sessions in the same environment and comparing them across the two environments, we revealed a double dissociation between the effects of time and experience on changes in activity rates and spatial tuning. Specifically, for both environments, ensemble rate correlations declined at similar rates when analyzed as a function of elapsed time between recording sessions, suggesting that changes in the overall activity levels of the individual cells are driven by the passage of time (Figures 3B, left, and S2B). Consistently, when the same data were analyzed in terms of the number of sessions in between two given visits in each environment, the correlations declined at a different rate (Figure 3B, right). Namely, the correlations across visits separated by the same number of sessions were lower for the environment visited every 4 days (environment B) than for the environment visited every 2 days (environment A). For instance, for a gap of 5 sessions, the ensemble rate correlations were lower for environment B, in which this gap corresponded to 20 days (Figure 3B, right, red curve), than for environment A, in which this gap corresponded to 10 days (Figure 3B, right, blue curve).

By contrast, the opposite effect was noted for changes in the spatial tuning of individual cells (Figures 3C and S2C). Specifically, for both environments, tuning curve correlations declined at similar rates when analyzed as a function of the number of sessions in between visits (Figure 3C, right), suggesting that changes in spatial tuning are driven by experience. Indeed, tuning curve correlations declined at a different rate across the two environments when the same data were analyzed as a function of elapsed time (Figure 3C, left). Namely, for a given temporal gap, the correlations from environment A were lower than those from environment B. For instance, for a gap of 12 days, there were lower tuning curve correlations for environment A, in which this gap corresponded to 6 sessions (Figure 3C, left, blue curve) than those of environment B, in which this gap corresponded to 3 sessions (Figure 3C, left, red curve). Using the population vector (PV) correlation (Figure 3A),[22–24] we found experience-dependent changes in the neuronal code at the population level

Please cite this article in press as: Geva et al., Time and experience differentially affect distinct aspects of hippocampal representational drift, Neuron (2023), https://doi.org/10.1016/j.neuron.2023.05.005

CellPress

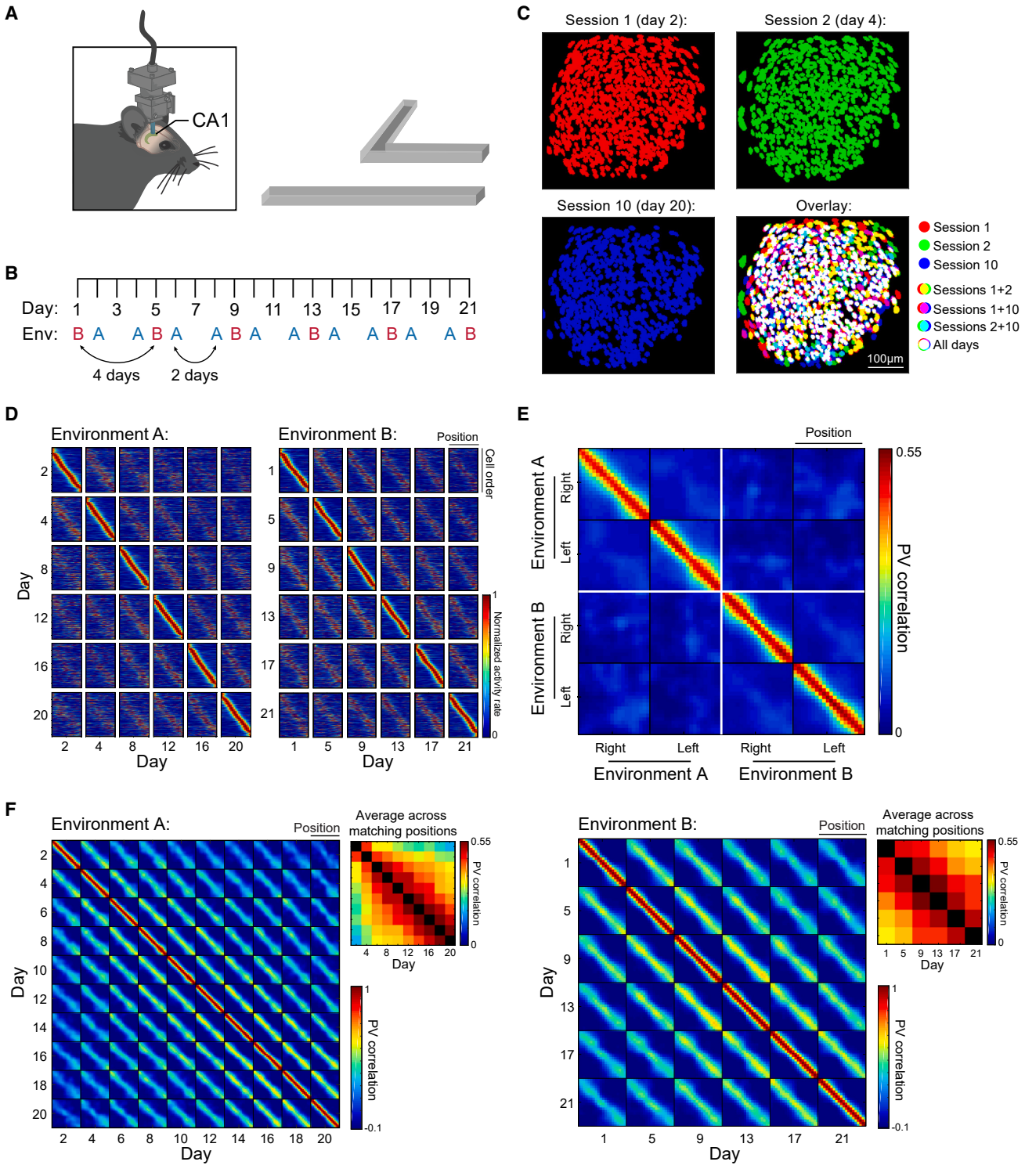

Figure 2. Spatial representations of familiar environments in hippocampal CA1 undergo representational drift over weeks

(A) Mice repeatedly explored two familiar linear tracks (right) while the Ca^{2+} activity of neurons in their CA1 was longitudinally recorded using a miniature microscope (left).

(B) Experimental timeline. Mice visited one of the two linear environments every 2 days (environment A, blue) and the other environment every 4 days (environment B, red).

(legend continued on next page)

Please cite this article in press as: Geva et al., Time and experience differentially affect distinct aspects of hippocampal representational drift, Neuron (2023), https://doi.org/10.1016/j.neuron.2023.05.005

(Figures 3D and S2D) that were qualitatively similar to those observed in spatial tuning at the single-cell level (Figure S3). Overall, our results suggest that the passage of time drives changes in activity rates and that experience drives changes in spatial tuning.[21–23]

In this experiment, mice were trained to obtain rewards at the ends of the linear tracks, thereby associating specific locations with rewards. The effects of time and experience persisted even when restricting our analysis only to the reward locations (Figures S1I and S1J), indicating that these salient locations undergo similar representational drift to the rest of the environment.

To rule out the possibility that differences in the number of registered recording sessions (10 recording sessions for environment A and 6 recording sessions for environment B) affected the results, we analyzed subsets of sessions from the two environments that had the same number of sessions or the same time gap between visits. The data from these subsets showed a similar trend to those of the full dataset (Figure S1K), indicating that differences in the number of sessions used for cell registration did not affect our results.

Our finding that neuronal activity rates and spatial tuning are differentially affected by time and experience raises the question of whether these aspects of representational drift are related. We found that session-to-session changes in activity rates were almost completely independent of changes in tuning curves (Figures S1L, S1M, and S1O). Similarly, the mean activity rate of individual cells across subsequent sessions explained only a small fraction of the variance in changes to the tuning curve of the same cells between these sessions (Figures S1N and S1O). Thus, there seems to be very little correspondence between the changes in activity rates and the changes in spatial tuning across sessions.

The finding that experience drives changes in neuronal representations (namely, the more experience the mouse had in the environment, the more changes in spatial tuning occurred) raises the question of whether and to what extent the experience that drives representational drift is context specific. Namely, whether experience in one environment contributes to the observed drift in the other environment. To address this question, we compared the similarity in the neuronal representations across two sets of pairs of consecutive sessions in environment A: those with an intermediate experience in environment B and those without an intermediate experience in environment B (Figure 2B). This analysis revealed no differences between the two types of session pairs in all three similarity measures (Figures 3E–3G). Notably, the experience-driven drift in spatial tuning was context specific, although the two contexts (environment A and environment B) shared numerous key features (e.g., both environments were linear tracks of the same length, and the temporal structure of the session in both environments was identical). Together, these results demonstrate that experience-driven drift in hippocampal codes is context specific.[15]

Recent studies have demonstrated that behavioral variability could contribute to representational changes,[25–29] highlighting the need to carefully control for behavioral factors in analyzing neural code stability. We analyzed the mice's behavior during repeated visits to the same environments and found that mice typically displayed a highly consistent behavior across sessions (Figures S4A–S4E), as expected, given the extensive pre-training and familiarization of the mice with the two linear track environments. To further exclude the possibility that our results stem from variability in behavioral performance across sessions and environments (e.g., number of track traversals), we repeated the analysis presented in Figures 3B–3D after subsampling the data, using the same number of traversals for all sessions in both environments. This analysis yielded similar results to those obtained with the complete dataset (Figure S4F). Moreover, we quantified how much of the variance observed in the three code similarity measures (ensemble rate correlations, tuning curve correlations, and PV correlations) was explained by time, experience, and various behavioral factors: running speed, number of traversals, occupancy profile, and velocity profile. For all code similarity measures, the values of explained variance for time or experience were at least 3–6 times greater than the values of the behavioral factors (Figure S4G). Together, these analyses suggest that our findings were not a result of behavioral variability.

Finally, we sought to characterize the observed changes in cells' spatial tuning in greater detail. Although some cells displayed highly similar tuning curves across days (e.g., cells 1–3 and 7–9 in Figure 4A), others showed gradual changes in the shape of their tuning curve (e.g., cells 4–6 and 10–12 in Figure 4A). To quantify these changes, we considered three types of alterations in spatial tuning in individual cells: (1) a shift in the cells' preferred position, (2) changes in the number of place fields, and (3) changes in the place-field size. We found that place cells showed a gradual experience-dependent change in their preferred position (Figures 4B–4D). However, we did not find a clear gradual change in the number (Figure 4E) or the size (Figure 4F) of the place fields of each cell. Together, these analyses suggest that the observed changes in spatial tuning (Figure 3C) are mostly characterized by shifts in existing place fields rather than by changes in the number or size of these fields.

DISCUSSION

Time and experience are two factors that have been assumed to profoundly affect memory representations. Here, we

(C) An example of a field of view showing cellular footprints from three sessions of Ca^{2+} imaging (sessions 1, 2, and 10) in the same animal, and an overlay of the aligned cell footprints from these sessions (indicated in red, green, and blue, respectively).
(D) The spatial tuning curve of the same cells across 6 recording days in each environment. Cells were pooled across all mice (n = 8) and ordered based on their primary place-field position on each reference session (i.e., rows). For visualization purposes, the tuning curve of each cell in each day was normalized relative to the spatial bin with the maximal activity on that day.
(E) Population vector (PV) correlations across all spatial locations, running directions, and environments averaged over all session pairs and mice (n = 8).
(F) PV correlations between the representations of different locations (pooled from both running directions) across 10 recording days in environment A (left) and 6 recording days in environment B (right), averaged over all mice (n = 8). Insets: PV correlations across recording days averaged across matching positions.

Please cite this article in press as: Geva et al., Time and experience differentially affect distinct aspects of hippocampal representational drift, Neuron (2023), https://doi.org/10.1016/j.neuron.2023.05.005

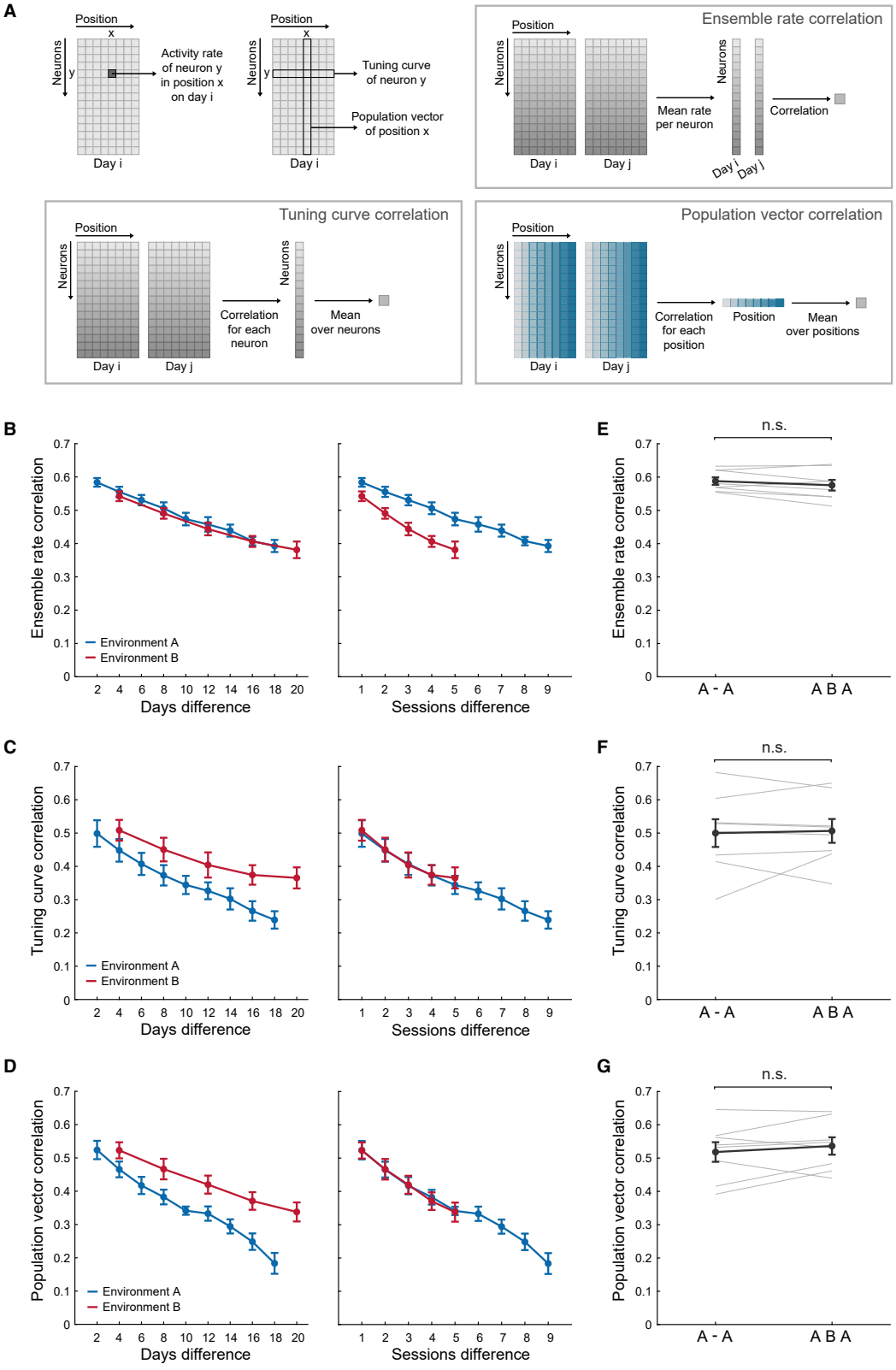

(legend on next page)

Please cite this article in press as: Geva et al., Time and experience differentially affect distinct aspects of hippocampal representational drift, Neuron (2023), https://doi.org/10.1016/j.neuron.2023.05.005

investigated how they affect hippocampal representational drift in familiar environments. We found a double dissociation between the absolute passage of time and the amount of experience in their impact on distinct aspects of code stability: time drives day-to-day changes in neuronal activity rates, whereas experience drives changes in spatial tuning. Although the exact mechanisms that drive and restrict drift are still unknown, this double dissociation suggests that different mechanisms govern different aspects of representational drift. For example, time-dependent drift in activity rates could be driven by changes in cells' excitability. Such changes may be intrinsic (e.g., fluctuations in the expression of specific ion channels or transcription factors[30]) or extrinsic (e.g., fluctuations in the activity of inhibitory interneurons[31]). Drift in spatial tuning may be driven by changes in synaptic connectivity, which could be mediated by changes in synaptic strength[32] or turnover in dendritic spines.[33] The effects of time and experience on hippocampal representational drift found here over timescales of days–weeks may differ for shorter timescales (minutes–hours).[34]

Our finding that time drives changes in activity rates is consistent with previous work showing context-independent gradual changes in spatial representations over days–weeks.[4] Specifically, gradual changes in the propensity of individual cells to be active are shared even across episodes or contexts with distinct neuronal representations (e.g., across environments for which hippocampal place cells have completely different place fields). Unlike changes in spatial tuning, which are (by definition) context specific, changes in neuronal activity levels are an aspect of representational drift that can well serve as a mechanism for context-independent timestamping. Namely, it allows the inference of the temporal relationship between experienced events by creating a link between events that occurred close in time and dissociating between temporally distant events.[4,5] Importantly, the propensity of individual cells to be active plays a role in determining the identity of the cells that are allocated to the representations of novel experiences,[16,35,36] and gradual changes in this propensity affect memory linking.[5] Thus, gradual changes in neuronal activity rates are important for memory at the behavioral level.

By contrast, changes in spatial tuning were unaffected by the passage of time itself but instead were driven specifically by experience in the same spatial context. The finding that experience-dependent drift is context specific is surprising because recent work has suggested that representational drift in a given context is driven by experience in other contexts.[6,14] Moreover, given that the representations of the different environments are carried by the same set of neurons that are connected by the same set of synapses, it is not trivial that biologically plausible plasticity rules would allow experience to drive changes specific to one representation while not affecting the other.[37–40]

Interestingly, the effect of experience on changes in neuronal tuning varies across brain areas. For example, in the primary olfactory cortex, daily exposure to familiar odors significantly reduces the rate of drift in tuning relative to that of repeated exposure every 8 days to the same familiar odors.[14] In the primary visual cortex, the representational drift in cells' tuning was found to persist over weeks, with or without repeated presentation of the same stimulus in the interim.[11] Thus, repeated exposure to the same stimulus can either increase (hippocampus), decrease (piriform cortex), or have no apparent effect (visual cortex) on the rate of representational drift in the cells' tuning beyond what is accounted for by the absolute passage of time. These seemingly contradictory findings make sense when considering the distinct function of each brain area and its role in memory. They further suggest a role for circuit architecture in permitting and restricting the drift. In sensory memory, the identity of the stimulus is the key element that is being represented and, as such, the repeated experience should be associated with a stable neural representation. In episodic memory, however, the memory is of the (holistic) events themselves. Therefore, every additional experience in a given context has a unique component, which is reflected as changes in the content and the code of the memory. Accordingly, experience-dependent changes in spatial tuning can be

Figure 3. Changes in neuronal activity rates are time-dependent, whereas changes in spatial tuning are experience-dependent

(A) Workflow for calculating the ensemble rate correlation (top right), tuning curve correlation (bottom left), and population vector (PV) correlation (bottom right).

(B) Ensemble rate correlations between recording sessions with a different number of separating days (left) or sessions (right). In both environments, ensemble rate correlations showed a significant gradual decrease as a function of elapsed time ($\chi^2_{(8)} = 64.89$, $p < 10^{-10}$ for environment A; $\chi^2_{(4)} = 30.50$, $p < 10^{-5}$ for environment B; Skillings-Mack test). Changes in ensemble rate correlations were similar between the two environments with respect to the elapsed time between sessions (left, $\chi^2_{(1)} = 1.05$, $p = 0.303$, Skillings-Mack test) but were different with respect to the amount of experience between them (right, $\chi^2_{(1)} = 23.04$, $p < 10^{-5}$, Skillings-Mack test).

(C) Tuning curve correlations between recording days with a different number of separating days (left) or sessions (right). In both environments, tuning curve correlations showed a significant gradual decrease as a function of elapsed time ($\chi^2_{(8)} = 66.36$, $p < 10^{-10}$ for environment A; $\chi^2_{(4)} = 25.7$, $p < 10^{-4}$ for environment B; Skillings-Mack test). Changes in tuning curve correlations were similar between the two environments with respect to the amount of experience between sessions (right, $\chi^2_{(1)} = 0.19$, $p = 0.657$, Skillings-Mack test) but were different with respect to the elapsed time between them (left, $\chi^2_{(1)} = 6.09$, $p = 0.0135$, Skillings-Mack test).

(D) PV correlations between recording days with a different number of separating days (left) or sessions (right). In both environments, PV correlations showed a significant gradual decrease as a function of elapsed time ($\chi^2_{(8)} = 65.81$, $p < 10^{-10}$ for environment A; $\chi^2_{(4)} = 28.60$, $p < 10^{-5}$ for environment B; Skillings-Mack test). The PV correlations were similar between the two environments with respect to the amount of experience between sessions (right, $\chi^2_{(1)} = 0.34$, $p = 0.554$, Skillings-Mack test) but were different with respect to the elapsed time between them (left, $\chi^2_{(1)} = 10.08$, $p = 0.0015$, Skillings-Mack test).

(E–G) Experience-dependent representational drift is context-specific. Mean ensemble rate correlations (E), tuning curve correlations (F), and PV correlations (G) between the representations of two types of pairs of consecutive sessions in environment A: session pairs with an intermediate experience in environment B ("A B A"; right) and session pairs without an intermediate experience in environment B ("A-A"; left), plotted for each mouse (gray lines) and for the mean ± SEM across mice (black line). No significant difference was observed in the ensemble rate ($W = 27$, $p = 0.250$; two-tailed Wilcoxon signed-rank test), tuning curve ($W = 19$, $p = 0.945$; two-tailed Wilcoxon signed-rank test), or PV ($W = 10$, $p = 0.312$; two-tailed Wilcoxon signed-rank test) correlations. In all relevant panels, data are mean ± SEM across mice.

Please cite this article in press as: Geva et al., Time and experience differentially affect distinct aspects of hippocampal representational drift, Neuron (2023), https://doi.org/10.1016/j.neuron.2023.05.005

CellPress

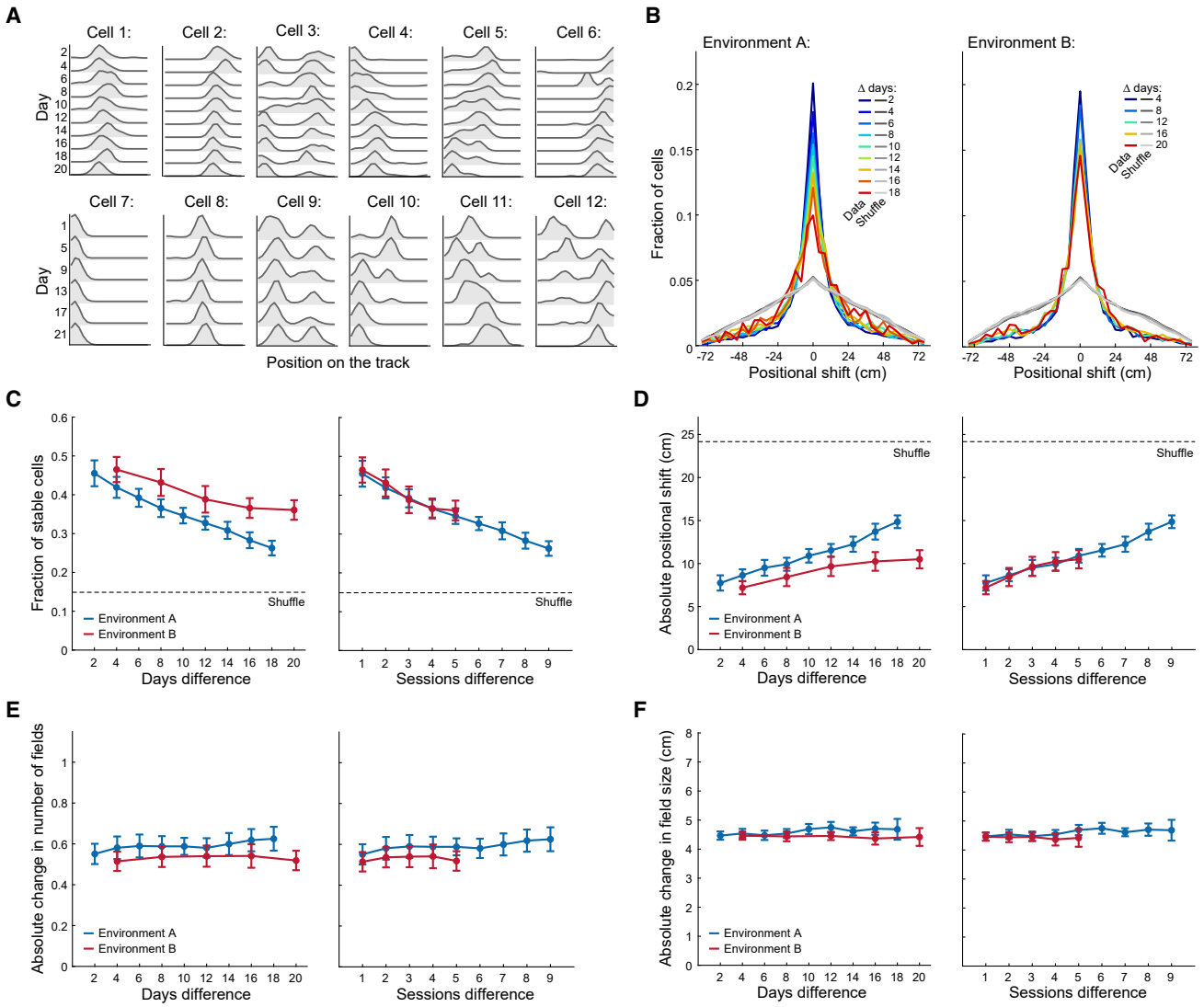

Figure 4. Shifts of existing place fields, rather than changes in their number or size, underly drift in spatial tuning

(A) Neuronal responses of 12 example cells showing varying degrees of tuning curve stability across days (cells 1–6 in environment A and cells 7–12 in environment B). For visualization purposes, the tuning curve of each cell in each day was normalized relative to the spatial bin with the maximal activity of that day.

(B) Distribution of place-field positional shifts for pairs of sessions in environment A (left) and environment B (right) showing place-field stability over long time periods (colored lines) relative to shuffled data in which the identity of the cells was intermixed independently within each day (gray lines). Note that in both environments, the fraction of cells that remained stable (i.e., place cells retaining their primary place field within ±4 cm between compared sessions of the same environment) gradually decreased as the time interval between sessions increased (from blue for short intervals to red for longer intervals).

(C) The percentage of stable place cells for recording sessions with a different number of separating days (left) or sessions (right) relative to shuffled data in which the identity of the cells was intermixed independently within each day (dashed line). In both environments, the fraction of cells that remained stable gradually decreased as a function of elapsed time ($\chi^2_{(8)} = 61.78$, $p < 10^{-9}$ for environment A; $\chi^2_{(4)} = 24.90$, $p < 10^{-4}$ for environment B; Skillings-Mack test). Changes in the fraction of stable cells were similar between the two environments with respect to the amount of experience between sessions (right, $\chi^2_{(1)} = 0.08$, $p = 0.767$, Skillings-Mack test) but were different with respect to the elapsed time between them (left, $\chi^2_{(1)} = 7.23$, $p = 0.007$, Skillings-Mack test).

(D) Absolute positional shift in place cells' primary place field between recording sessions with a different number of separating days (left) or sessions (right) relative to shuffled data in which the identity of the cells was intermixed independently within each day (dashed line). In both environments, place cells showed a significant gradual increase in the positional shift of their primary place field as a function of elapsed time ($\chi^2_{(8)} = 43.72$, $p < 10^{-6}$ for environment A; $\chi^2_{(4)} = 21.02$, $p < 10^{-3}$ for environment B; Skillings-Mack test). Changes in the field's positional shift were similar between the two environments with respect to the amount of experience between sessions (left, $\chi^2_{(1)} = 0.49$, $p = 0.482$, Skillings-Mack test) but were different with respect to the elapsed time between them (right, $\chi^2_{(1)} = 5.63$, $p = 0.017$, Skillings-Mack test).

(E) Absolute change in the number of place fields per place cell between recording sessions with a different number of separating days (left) or sessions (right). In both environments, the number of place fields per place cell did not significantly change as a function of elapsed time ($\chi^2_{(8)} = 6.75$, $p = 0.563$ for environment A; $\chi^2_{(4)} = 2.70$, $p = 0.609$ for environment B; Skillings-Mack test). Changes in the number of place fields per place cell were similar between the two environments,

(legend continued on next page)

thought of as a manifestation of re-consolidation processes at the neural code level.[41,42] Such processes may benefit memory by allowing memories to be continuously updated.[7,43]

Although it remains to be studied whether drift along different dimensions of coding stability has a qualitatively different impact on memory function, it stands to reason that the existence of drift (and specifically of changes in the tuning curves; Figures S3E and S3F) would pose a challenge for a downstream circuit, unless some mechanisms that restrict the drift (e.g., restricting it to non-coding dimensions[6,44]) or adjust the downstream circuits to it are involved. Indeed, recent theoretical studies have suggested several biologically plausible solutions for this problem.[45–47] For instance, certain plasticity rules may allow significant changes in neuronal representations while preserving the network's functionality by maintaining a stable structure of relationships between these neuronal representations.[47] These theoretical predictions are consistent with recent experimental data from the hippocampus and visual cortex, showing that the structure of relationships between internal representations persists over time despite the drift in the tuning and activity rates of individual neurons.[4,10,48,49]

In summary, our work deconstructs representational drift into two key components that are differentially affected by two key factors that affect long-term memory. As such, our findings will help to inform future experimental and theory-based efforts to reveal the mechanisms and functional implications of representational drift and suggest that such endeavors should avoid considering drift as a unitary phenomenon and instead view it as a multi-faceted process supported by distinct neuronal mechanisms that could play different roles in hippocampal function and memory.

STAR★METHODS

Detailed methods are provided in the online version of this paper and include the following:

- KEY RESOURCES TABLE
- RESOURCE AVAILABILITY
  - Lead contact
  - Materials availability
  - Data and code availability
- EXPERIMENTAL MODEL AND SUBJECT DETAILS
  - Animals
- METHOD DETAILS
  - Surgical procedures
  - Ca^{2+} imaging and behavioral setup
  - Mouse position tracking
  - Processing Ca^{2+} imaging data
  - Detection of Ca^{2+} events
  - Registration of cells across sessions
  - Place cell identification
  - Population vector correlation
  - Ensemble rate correlation
  - Tuning curve correlation
  - Relationship between activity rate and tuning curve stability (related to Figures S1L–S1O)
  - Place fields characterization (related to Figures 4B–4F and S1E–S1G)
  - Simulating representational drift (related to Figure S3)
  - Stability of occupancy and velocity profiles (related to Figures S4D and S4E)
  - Controlling for task performance variability (related to Figure S4F)
  - Relationship between neuronal code stability and behavioral variability (related to Figure S4G)
  - Statistical analysis

SUPPLEMENTAL INFORMATION

Supplemental information can be found online at https://doi.org/10.1016/j.neuron.2023.05.005.

ACKNOWLEDGMENTS

Y.Z. is head of the Mike and Valeria Rosenbloom Center for Positive Neuroscience and is supported by grants from the Belle S. and Irving E. Meller Center for the Biology of Aging, European Research Council (ERC-CoG 101001226), Human Frontier Science Program (RGY0069/2017), and Israel Science Foundation (2113/19). We thank Sasha Devore, Liron Sheintuch, Gal Elyasaf, Itay Talpir, Ofri Axelrod, Nitzan Shalvi, and Eda Montalieu for helpful advice and comments on the manuscript.

AUTHOR CONTRIBUTIONS

N.G., A.R., and Y.Z. conceived the project. N.G. conducted the experiments. N.G. and D.D. analyzed the data. N.G., D.D., A.R., and Y.Z. wrote and revised the manuscript. A.R. and Y.Z. supervised the research. Y.Z. obtained funding.

DECLARATION OF INTERESTS

The authors declare no competing interests.

Received: September 22, 2022
Revised: February 22, 2023
Accepted: May 8, 2023
Published: June 13, 2023

REFERENCES

1. Manns, J.R., Howard, M.W., and Eichenbaum, H. (2007). Gradual changes in hippocampal activity support remembering the order of events. Neuron *56*, 530–540. https://doi.org/10.1016/j.neuron.2007.08.017.
2. Mankin, E.A., Sparks, F.T., Slayyeh, B., Sutherland, R.J., Leutgeb, S., and Leutgeb, J.K. (2012). Neuronal code for extended time in the

both with respect to the elapsed time between sessions (left, $\chi^2_{(1)} = 0.32$, $p = 0.566$, Skillings-Mack test) and with respect to the amount of experience between them (right, $\chi^2_{(1)} = 0.13$, $p = 0.711$, Skillings-Mack test).
(F) Absolute change in place cells' primary place-field size between recording sessions with a different number of separating days (left) or sessions (right). In both environments, the size of the primary place field of the same cells did not significantly change as a function of elapsed time ($\chi^2_{(8)} = 10.21$, $p = 0.250$ for environment A; $\chi^2_{(4)} = 0.70$, $p = 0.951$ for environment B; Skillings-Mack test). Changes in the primary place-field size were similar between the two environments, both with respect to the elapsed time between sessions (left, $\chi^2_{(1)} = 0.60$, $p = 0.435$, Skillings-Mack test) and with respect to the amount of experience between them (right, $\chi^2_{(1)} = 0.04$, $p = 0.824$, Skillings-Mack test). In (C)–(F), data are mean ± SEM across mice.

hippocampus. Proc. Natl. Acad. Sci. USA *109*, 19462–19467. https://doi.org/10.1073/pnas.1214107109.

3. Ziv, Y., Burns, L.D., Cocker, E.D., Hamel, E.O., Ghosh, K.K., Kitch, L.J., el Gamal, A., and Schnitzer, M.J. (2013). Long-term dynamics of CA1 hippocampal place codes. Nat. Neurosci. *16*, 264–266. https://doi.org/10.1038/nn.3329.
4. Rubin, A., Geva, N., Sheintuch, L., and Ziv, Y. (2015). Hippocampal ensemble dynamics timestamp events in long-term memory. eLife *4*, e12247. https://doi.org/10.7554/eLife.12247.
5. Cai, D.J., Aharoni, D., Shuman, T., Shobe, J., Biane, J., Song, W., Wei, B., Veshkini, M., La-Vu, M., Lou, J., et al. (2016). A shared neural ensemble links distinct contextual memories encoded close in time. Nature *534*, 115–118. https://doi.org/10.1038/nature17955.
6. Rule, M.E., O'Leary, T., and Harvey, C.D. (2019). Causes and consequences of representational drift. Curr. Opin. Neurobiol. *58*, 141–147. https://doi.org/10.1016/j.conb.2019.08.005.
7. Driscoll, L.N., Duncker, L., and Harvey, C.D. (2022). Representational drift: emerging theories for continual learning and experimental future directions. Curr. Opin. Neurobiol. *76*, 102609. https://doi.org/10.1016/J.CONB.2022.102609.
8. Masset, P., Qin, S., and Zavatone-Veth, J.A. (2022). Drifting neuronal representations: bug or feature? Biol. Cybern. *116*, 253–266. https://doi.org/10.1007/s00422-021-00916-3.
9. Driscoll, L.N., Pettit, N.L., Minderer, M., Chettih, S.N., and Harvey, C.D. (2017). Dynamic reorganization of neuronal activity patterns in parietal cortex. Cell *170*, 986–999.e16. https://doi.org/10.1016/j.cell.2017.07.021.
10. Deitch, D., Rubin, A., and Ziv, Y. (2021). Representational drift in the mouse visual cortex. Curr. Biol. *31*, 4327–4339.e6. https://doi.org/10.1016/j.cub.2021.07.062.
11. Marks, T.D., and Goard, M.J. (2021). Stimulus-dependent representational drift in primary visual cortex. Nat. Commun. *12*, 5169. https://doi.org/10.1038/s41467-021-25436-3.
12. Aschauer, D.F., Eppler, J.-B., Ewig, L., Chambers, A.R., Pokorny, C., Kaschube, M., and Rumpel, S. (2022). Learning-induced biases in the ongoing dynamics of sensory representations predict stimulus generalization. Cell Rep. *38*, 110340. https://doi.org/10.1016/j.celrep.2022.110340.
13. Wang, H.C., LeMessurier, A.M., and Feldman, D.E. (2022). Tuning instability of non-columnar neurons in the salt-and-pepper whisker map in somatosensory cortex. Nat. Commun. *13*, 6611. https://doi.org/10.1038/s41467-022-34261-1.
14. Schoonover, C.E., Ohashi, S.N., Axel, R., and Fink, A.J.P. (2021). Representational drift in primary olfactory cortex. Nature *594*, 541–546. https://doi.org/10.1038/s41586-021-03628-7.
15. Keinath, A.T., Mosser, C.-A., and Brandon, M.P. (2022). The representation of context in mouse hippocampus is preserved despite neural drift. Nat. Commun. *13*, 2415. https://doi.org/10.1038/s41467-022-30198-7.
16. Lee, J.S., Briguglio, J.J., Cohen, J.D., Romani, S., and Lee, A.K. (2020). The statistical structure of the hippocampal code for space as a function of time, context, and value. Cell *183*, 620–635.e22. https://doi.org/10.1016/j.cell.2020.09.024.
17. Hainmueller, T., and Bartos, M. (2018). Parallel emergence of stable and dynamic memory engrams in the hippocampus. Nature *558*, 292–296. https://doi.org/10.1038/s41586-018-0191-2.
18. Mau, W., Sullivan, D.W., Kinsky, N.R., Hasselmo, M.E., Howard, M.W., and Eichenbaum, H. (2018). The same hippocampal CA1 population simultaneously codes temporal information over multiple timescales. Curr. Biol. *28*, 1499–1508.e4. https://doi.org/10.1016/j.cub.2018.03.051.
19. Sheintuch, L., Rubin, A., Brande-Eilat, N., Geva, N., Sadeh, N., Pinchasof, O., and Ziv, Y. (2017). Tracking the same neurons across multiple days in Ca2+ imaging data. Cell Rep. *21*, 1102–1115. https://doi.org/10.1016/j.celrep.2017.10.013.
20. Muller, R.U., and Kubie, J.L. (1987). The effects of changes in the environment on the spatial firing of hippocampal complex-spike cells. J. Neurosci. *7*, 1951–1968. https://doi.org/10.1523/JNEUROSCI.07-07-01951.1987.
21. Fyhn, M., Hafting, T., Treves, A., Moser, M.B., and Moser, E.I. (2007). Hippocampal remapping and grid realignment in entorhinal cortex. Nature *446*, 190–194. https://doi.org/10.1038/nature05601.
22. Pastalkova, E., Itskov, V., Amarasingham, A., and Buzsáki, G. (2008). Internally generated cell assembly sequences in the rat hippocampus. Science *321*, 1322–1327. https://doi.org/10.1126/science.1159775.
23. Leutgeb, S., Leutgeb, J.K., Barnes, C.A., Moser, E.I., McNaughton, B.L., and Moser, M.B. (2005). Independent codes for spatial and episodic memory in hippocampal neuronal ensembles. Science *309*, 619–623. https://doi.org/10.1126/science.1114037.
24. Sheintuch, L., Geva, N., Baumer, H., Rechavi, Y., Rubin, A., and Ziv, Y. (2020). Multiple maps of the same spatial context can stably coexist in the mouse hippocampus. Curr. Biol. *30*, 1467–1476.e6. https://doi.org/10.1016/j.cub.2020.02.018.
25. Stringer, C., Pachitariu, M., Steinmetz, N., Reddy, C.B., Carandini, M., and Harris, K.D. (2019). Spontaneous behaviors drive multidimensional, brain-wide activity. Science *364*, 255. https://doi.org/10.1126/science.aav7893.
26. Musall, S., Kaufman, M.T., Juavinett, A.L., Gluf, S., and Churchland, A.K. (2019). Single-trial neural dynamics are dominated by richly varied movements. Nat. Neurosci. *22*, 1677–1686. https://doi.org/10.1038/s41593-019-0502-4.
27. Liberti, W.A., Schmid, T.A., Forli, A., Snyder, M., and Yartsev, M.M. (2022). A stable hippocampal code in freely flying bats. Nature *604*, 98–103. https://doi.org/10.1038/s41586-022-04560-0.
28. Sadeh, S., and Clopath, C. (2022). Contribution of behavioural variability to representational drift. eLife *11*, e77907. https://doi.org/10.7554/eLife.77907.
29. Jensen, K.T., Kadmon Harpaz, N., Dhawale, A.K., Wolff, S.B.E., and Ölveczky, B.P. (2022). Long-term stability of single neuron activity in the motor system. Nat. Neurosci. *25*, 1664–1674. https://doi.org/10.1038/s41593-022-01194-3.
30. Silva, A.J., Kogan, J.H., Frankland, P.W., and Kida, S. (1998). CREB and memory. Annu. Rev. Neurosci. *21*, 127–148. https://doi.org/10.1146/annurev.neuro.21.1.127.
31. Lapray, D., Lasztoczi, B., Lagler, M., Viney, T.J., Katona, L., Valenti, O., Hartwich, K., Borhegyi, Z., Somogyi, P., and Klausberger, T. (2012). Behavior-dependent specialization of identified hippocampal interneurons. Nat. Neurosci. *15*, 1265–1271. https://doi.org/10.1038/nn.3176.
32. Hayashi, Y. (2019). NMDA receptor-dependent dynamics of hippocampal place cell ensembles. J. Neurosci. *39*, 5173–5182. https://doi.org/10.1523/JNEUROSCI.0243-19.2019.
33. Attardo, A., Fitzgerald, J.E., and Schnitzer, M.J. (2015). Impermanence of dendritic spines in live adult CA1 hippocampus. Nature *523*, 592–596. https://doi.org/10.1038/nature14467.
34. Khatib, D., Ratzon, A., Sellevoll, M., Barak, O., Morris, G., and Derdikman, D. (2023). Active experience, not time, determines within day representational drift in dorsal CA1. Neuron *111*. https://doi.org/10.1016/j.neuron.2023.05.014.
35. Yiu, A.P., Mercaldo, V., Yan, C., Richards, B., Rashid, A.J., Hsiang, H.L.L., Pressey, J., Mahadevan, V., Tran, M.M., Kushner, S.A., et al. (2014). Neurons are recruited to a memory trace based on relative neuronal excitability immediately before training. Neuron *83*, 722–735. https://doi.org/10.1016/j.neuron.2014.07.017.
36. Rashid, A.J., Yan, C., Mercaldo, V., Hsiang, H.L., Park, S., Cole, C.J., De Cristofaro, A., Yu, J., Ramakrishnan, C., Lee, S.Y., et al. (2016). Competition between engrams influences fear memory formation and recall. Science *353*, 383–387. https://doi.org/10.1126/science.aaf0594.
37. Hopfield, J.J. (1982). Neural networks and physical systems with emergent collective computational abilities. Proc. Natl. Acad. Sci. USA *79*, 2554–2558. https://doi.org/10.1073/pnas.79.8.2554.

38. McCloskey, M., and Cohen, N.J. (1989). Catastrophic interference in connectionist networks: the sequential learning problem. Phychol. Learn. Motiv. *24*, 109–165. https://doi.org/10.1016/S0079-7421(08)60536-8.

39. Haviv, D., Rivkind, A., and Barak, O. (2019). Understanding and controlling memory in recurrent neural networks. https://doi.org/10.48550/arXiv.1902.07275.

40. Masse, N.Y., Grant, G.D., and Freedman, D.J. (2018). Alleviating catastrophic forgetting using context-dependent gating and synaptic stabilization. Proc. Natl. Acad. Sci. USA *115*, E10467–E10475. https://doi.org/10.1073/pnas.1803839115.

41. Dudai, Y. (2012). The restless engram: consolidations never end. Annu. Rev. Neurosci. *35*, 227–247. https://doi.org/10.1146/annurev-neuro-062111-150500.

42. Nader, K., and Hardt, O. (2009). A single standard for memory: the case for reconsolidation. Nat. Rev. Neurosci. *10*, 224–234. https://doi.org/10.1038/nrn2590.

43. Mau, W., Hasselmo, M.E., and Cai, D.J. (2020). The brain in motion: how ensemble fluidity drives memory-updating and flexibility. eLife *9*, e63550. https://doi.org/10.7554/eLife.63550.

44. Rule, M.E., Loback, A.R., Raman, D.V., Driscoll, L.N., Harvey, C.D., and O'Leary, T. (2020). Stable task information from an unstable neural population. eLife *9*, e51121. https://doi.org/10.7554/eLife.51121.

45. Kossio, Y.F.K., Goedeke, S., Klos, C., and Memmesheimer, R.-M. (2021). Drifting assemblies for persistent memory: neuron transitions and unsupervised compensation. Proc. Natl. Acad. Sci. USA *118*, e2023832118. https://doi.org/10.1073/pnas.2023832118.

46. Rule, M.E., and O'Leary, T. (2022). Self-healing codes: how stable neural populations can track continually reconfiguring neural representations. Proc. Natl. Acad. Sci. USA *119*, e2106692119. https://doi.org/10.1073/pnas.2106692119.

47. Qin, S., Farashahi, S., Lipshutz, D., SenGupta, A.M., Chklovskii, D.B., and Pehlevan, C. (2023). Coordinated drift of receptive fields in Hebbian/anti-Hebbian network models during noisy representation learning. Nat. Neurosci. *26*, 339–349. https://doi.org/10.1038/s41593-022-01225-z.

48. Xia, J., Marks, T.D., Goard, M.J., and Wessel, R. (2021). Stable representation of a naturalistic movie emerges from episodic activity with gain variability. Nat. Commun. *12*, 5170. https://doi.org/10.1038/s41467-021-25437-2.

49. Rubin, A., Sheintuch, L., Brande-Eilat, N., Pinchasof, O., Rechavi, Y., Geva, N., and Ziv, Y. (2019). Revealing neural correlates of behavior without behavioral measurements. Nat. Commun. *10*, 4745. https://doi.org/10.1038/s41467-019-12724-2.

50. Dana, H., Chen, T.W., Hu, A., Shields, B.C., Guo, C., Looger, L.L., Kim, D.S., and Svoboda, K. (2014). Thy1-GCaMP6 transgenic mice for neuronal population imaging in vivo. PLoS One *9*, e108697. https://doi.org/10.1371/journal.pone.0108697.

51. Mukamel, E.A., Nimmerjahn, A., and Schnitzer, M.J. (2009). Automated analysis of cellular signals from large-scale calcium imaging data. Neuron *63*, 747–760. https://doi.org/10.1016/j.neuron.2009.08.009.

52. Markus, E.J., Barnes, C.A., McNaughton, B.L., Gladden, V.L., and Skaggs, W.E. (1994). Spatial information content and reliability of hippocampal CA1 neurons: effects of visual input. Hippocampus *4*, 410–421. https://doi.org/10.1002/hipo.450040404.

53. Rechavi, Y., Rubin, A., Yizhar, O., and Ziv, Y. (2022). Exercise increases information content and affects long-term stability of hippocampal place codes. Cell Rep. *41*, 111695. https://doi.org/10.1016/j.celrep.2022.111695.

54. Chatfield, M., and Mander, A. (2009). The skillings-mack test (Friedman test when there are missing data). STATA J. *9*, 299–305. https://doi.org/10.1177/1536867x0900900208.

Please cite this article in press as: Geva et al., Time and experience differentially affect distinct aspects of hippocampal representational drift, Neuron (2023), https://doi.org/10.1016/j.neuron.2023.05.005

STAR★METHODS

KEY RESOURCES TABLE

REAGENT or RESOURCE	SOURCE	IDENTIFIER
Chemicals, peptides, and recombinant proteins		
C&B Metabond	Parkell	S380
Ultraviolet-curing adhesive	Norland	NOA 81
Flow-It ALC	Pentron	Univ. Opaque
Deposited data		
Data to produce figures	This paper	https://doi.org/10.5281/zenodo.8010591
Experimental models: Organisms/strains		
Thy1-GCaMP6f (GP5.17Dkim/J)	The Jackson Laboratory	JAX: 025393
CD-1 (ICR)	Weizmann Institute	RRID:MGI:5652659
Software and algorithms		
Original code	This paper	https://doi.org/10.5281/zenodo.8010591
nVista Acquisition Software	Inscopix inc.	Version 2.0
Inscopix Data Acquisition Software	Inscopix inc.	Version 1.3
Inscopix Data Processing Software	Inscopix inc.	Version 1.4
Mosaic	Inscopix inc.	1.1.1b
IC Capture	The imaging source	Version 2.4
EthoVision XT	Noldus	Version 12.0
MATLAB (version 2014a and 2017b)	Mathworks	https://se.mathworks.com/products/matlab.html
CellReg – cell registration method	Sheintuch et al.[19]	https://github.com/zivlab/CellReg
Other		
Integrated miniature fluorescence microscope	Inscopix inc.	nVista 2.0 and nVista 3.0
Gradient refractive index (GRIN) lens	Inscopix inc.	Cat # 1050-002176
Inscopix commutator	Inscopix inc.	Version 1
Overhead camera for recording animal behavior	The imaging source	DFK 33G445

RESOURCE AVAILABILITY

Lead contact

Further information and requests should be directed to the lead contact, Yaniv Ziv (yaniv.ziv@weizmann.ac.il).

Materials availability

This study did not generate new unique reagents.

Data and code availability

- Data to reproduce the figures is available as of the date of publication at https://github.com/zivlab/time_vs_experience.
- All original code has been deposited at Zenodo and is publicly available as of the date of publication.
- Any additional information required to reanalyze the data reported in this paper will be available from the lead contact upon request.

EXPERIMENTAL MODEL AND SUBJECT DETAILS

Animals

All procedures were approved by the Weizmann Institute IACUC. Eight male, Thy1-GCaMP6f transgenic mice (Jackson stock number 025393; 4 with a C57BL/6 background and 4 with an ICR(CD-1) background), aged 3-6 months at the start of imaging, were used in this study.[50] Mice were housed with 1-3 cage-mates in cages with running wheels in a 12:12 hour reverse light cycle (lights off 10 am-10 pm).

Please cite this article in press as: Geva et al., Time and experience differentially affect distinct aspects of hippocampal representational drift, Neuron (2023), https://doi.org/10.1016/j.neuron.2023.05.005

METHOD DETAILS

Surgical procedures

We implanted all mice, under isoflurane anesthesia (1.5-2% volume), with a glass guide tube directly above the CA1. We used a trephine drill to remove a circular part of the skull above the hippocampus. We then removed the dura and cortex above the CA1 by suction with a 29-gauge blunt needle while constantly washing the exposed tissue with sterile phosphate-buffered saline (PBS). Next, we implanted an optical guide tube with its window just dorsal to, but not within, area CA1 and sealed the space between the skull and the guide tube using 1.5% agarose in PBS. The exposed skull areas were then sealed with Metabond (Parkell, Edgewood, NY) and dental acrylic. Mice were then allowed to recover for at least two weeks.

Ca^{2+} imaging and behavioral setup

Before we began Ca^{2+} imaging, mice were water-restricted and habituated to human handling by allowing them to walk on the experimenters' hands. At least three weeks after guide-tube implantation, mice were imaged under isoflurane anesthesia using a two-photon microscope (Ultima IV, Bruker, Germany). We inserted a microendoscope consisting of a single gradient refractive index lens (1 mm diameter, Inscopix) into the guide tube and examined Ca^{2+} indicator expression and tissue health. We selected for further imaging only those mice that exhibited homogenous GCaMP6f expression and appeared to have healthy tissue. For the selected mice, we then affixed the microendoscope within the guide tube using an ultraviolet-curing adhesive (Norland, NOA81, Edmund Optics, Barrington, NJ). Next, we attached the microscope's base plate to the dental acrylic cap using a light-cured adhesive (Flow-It ALC, Pentron, Orange, CA). To record mice behavior, we used an overhead camera (DFK 33G445, The Imaging Source, Germany), which we synchronized with the integrated microscope. Ca^{2+} imaging was performed at 10 Hz.

We performed time-lapse imaging in freely behaving mice using an integrated miniature fluorescence microscope (nVista, Inscopix). For 6 mice, we used nVista v2 systems, and for another 2 mice, we used nVista v3 with the commercial Inscopix commutator. Before starting the experiment, we accustomed the mice to the head-mounted microscopes and familiarized the mice with two linear tracks. In this pre-training phase, mice were trained to run back and forth to collect water rewards in each of the tracks over 6–9 days (at least 20 min/per session). The tracks differed in their geometry and had distinct sets of visual and tactile cues, overhead lights, and odor cues. One environment was a straight 96-cm-long track, while the other was an L-shaped track consisting of two 48-cm-long arms. Each environment had a separate set of curtains with different colors and patterns, which made up the walls of the recording enclosure (distal cues), and also had distinct visual cues scattered along the walls of each track (proximal cues). Before the beginning of each session, we wiped the tracks with differently scented paper towels (0.5% acetic acid for the straight track and 10% ethanol for the L-shaped track). The water reward was dispensed at both ends of the tracks using a custom-made computer-controlled device. Imaging sessions started after pre-training. Each imaging session consisted of two 10-minute-long trials, with an inter-trial interval (ITI) of 3 minutes, during which the mice were put in a clear circular plastic bucket, which was placed at a specific fixed position on top of the track. Special care was taken to ensure each mouse was placed on the track in the same way across all trials. Each mouse visited one environment every 2 days and the other every 4 days, for a total of 10 and 6 sessions, respectively. The mice were randomly assigned one of the two tracks (straight and L-shaped) and the frequency of visits: every 2 days (Environment A) or 4 days (Environment B). For five mice, the straight linear track was assigned as Environment A, and for three mice, the L-shaped track was assigned as Environment A.

Mouse position tracking

The position and velocity of the mouse were estimated using video tracking software (EthoVision XT 12) which detects the mouse's center of mass in each frame based on its pixels' intensity and shape, compared to a background image. The parameters used for the software were chosen manually for each behavioral video to ensure high annotation quality of the estimated position.

Processing Ca^{2+} imaging data

We processed the Ca^{2+} imaging data using commercial software (Mosaic, version 1.1.1b, or Inscopix Data Processing Software, version 1.4, Inscopix,) and custom MATLAB routines as previously described.[3,4,24] To increase the computation speed, we spatially down-sampled the data by a factor of four in each dimension (final pixel size of 2.5 X 2.5 μm). To correct for non-uniform illumination, both in space and in time, we normalized the images by dividing each pixel by the corresponding value from a smoothed image. The smoothed image was obtained by applying a Gaussian filter with a radius of 100 μm to the movies. Normalization also enhanced the appearance of blood vessels, which were later used as stationary fiducial markers for image registration. We used a rigid-body registration to correct for lateral displacements of the brain. This procedure was performed on a high-contrast sub-region of the normalized movies in which the blood vessels were most prominent. The movies were transformed into relative fluorescence changes, $\frac{\Delta F(t)}{F_0} = (F(t) - F_0)/F_0$, where F_0 is the value for each pixel averaged over the entire recording duration. For cell detection, the movies were down sampled in time by a factor of two. We detected spatial footprints corresponding to individual cells using an established cell-detection algorithm that applies principal and independent component analyses (PCA and ICA).[51] For each spatial footprint, we used a threshold of 50% of the footprint's maximum intensity, and each pixel that did not cross this threshold was set to zero. After the cells were detected, further cell sorting was performed to identify the spatial footprints that follow a typical cellular structure. This

Please cite this article in press as: Geva et al., Time and experience differentially affect distinct aspects of hippocampal representational drift, Neuron (2023), https://doi.org/10.1016/j.neuron.2023.05.005

was done by measuring the footprint area and circularity, discarding those whose radius was smaller than 5 μm or larger than 15 μm or which had a circularity smaller than 0.8. In some cases, the output of the PCA/ICA algorithm included more than one component that corresponded to a single cell. To eliminate such occurrences, we examined all pairs of cells with centroid distances <18 μm; whenever their traces had a correlation >0.9, the cell with the lower average event peak amplitude was discarded.

Detection of Ca^{2+} events

Ca^{2+} activity was extracted by applying the thresholded spatial footprints to the $\Delta F(t)/F_0$ Ca^{2+} movies at full temporal resolution (10 Hz). Baseline fluctuations were removed by subtracting the median trace (10 sec sliding window). The Ca^{2+} traces were smoothed with a low-pass filter with a cutoff frequency of 2 Hz. Ca^{2+} candidate events were detected whenever the amplitude crossed a threshold of 4 median absolute deviations (MAD). We considered for further analysis only candidate Ca^{2+} events with an indicator decay time equal to or longer than 600 ms. In order to avoid the detection of several peaks corresponding to a single Ca^{2+} event, only peaks 4 MAD higher than the previous peak (within the same candidate event) and 2 MAD higher than the next peak were regarded as true events. We set the Ca^{2+} event occurrence to the time of the peak fluorescence. To mitigate the effects of crosstalk (i.e., spillover of Ca^{2+} fluorescence from neighboring cells), we adopted a conservative approach, allowing only one cell from a group of neighbors (pairs of cells with centroid distances <18 μm) to register a Ca^{2+} event in any 200 msec time window. If multiple Ca^{2+} events occurred within ~200 msec in neighboring cells, we retained only the event with the highest peak $\Delta F(t)/F_0$ value. If two neighboring cells had a correlation >0.9 in their events, the cell with the lower average peak amplitude was discarded. After the events were identified, further event sorting was performed to find the cells with sufficient signal-to-noise ratios. This was done by measuring the event rate and the average event peak amplitude for each cell and discarding those whose event rate was smaller than 0.005 Hz or which had an average event amplitude smaller than 1% ($\Delta F(t)/F_0$).

Registration of cells across sessions

To identify the same neurons across multiple imaging sessions, we used a probabilistic method for cell registration.[19] This method models the distribution of spatial correlations and centroid distances for neighboring cells from different recording sessions (candidates for being the same cell) as a weighted sum of the distributions of two subpopulations: same cells and different cells. Then, based on the model that best fits the data, the method estimates the probability of each candidate in the dataset to be the same cell (P_{same}). This allows the estimation of the overall rates of false-positive errors (different cells falsely registered as the same cell) and false-negative errors (the same cell falsely registered as different cells), providing a P_{same} registration threshold that is optimized for the dataset of each mouse. The threshold used for registration controls the tradeoff between false-positive and false-negative errors. Therefore, we chose a registration threshold of P_{same}=0.5, which constitutes an appropriate balance between false-positive and false-negative registration errors.[19] Note that while some of the same-cell candidates had intermediate spatial correlation values, the vast majority of such cell pairs exhibited either very high spatial correlations (suggesting they are the same cell) or very low spatial correlations. In cases with multiple candidates that cross the registration threshold, only the pair with the highest P_{same} was registered as the same cell, thus avoiding some of the false-positive errors; the result of this action was lower percentages of false-positive errors than those estimated by the probabilistic model.

Place cell identification

We divided each track into 24 bins (4 cm each) and excluded the last 2 bins at both ends of the tracks where water rewards were consumed, and the mouse was generally stationary.[3] Then, we calculated the time spent in each bin and the number of Ca^{2+} events per bin, considering only periods when the mouse ran >2 cm/sec while separating the analysis between left and right running directions. Finally, we calculated the tuning curve for each neuron in each running direction by dividing the number Ca^{2+} events by the occupancy in each spatial bin. For each tuning curve with >3 events in a given session, we calculated the spatial information (in bits per event), as previously described:[52]

$$spatial\ information = \sum_i p_i (r_i / \bar{r}) log_2 (r_i / \bar{r}),$$

where r_i is the firing rate of the neuron in the i^{th} bin, p_i the probability of the mouse being in the i^{th} bin (time spent in i^{th} bin divided by the total session time), $\bar{r}$ the overall mean firing rate, and index i running over all the spatial bins. We then performed 1000 distinct random shuffles of animal locations, accounting for the spatial coverage statistics at the relevant session and running direction, and calculated the spatial information for each shuffle realization. This yielded the p-value of the measured information for each tuning curve relative to the information of its corresponding shuffled data. Cells with significantly informative tuning curves ($p<0.05$) were considered as place cells for further analysis.

Population vector correlation

To determine the degree of similarity between spatial representations across days, we calculated for each mouse the population vector correlation between pairs of sessions that either occurred in the same environment (Figures 2F, 3D, 3G, S2A, S2D, and S4F) or between pairs of sessions that occurred in different environments (Figures 2E and S1H).[23] First, we divided each track into 24 bins (4 cm each), and then calculated for each spatial bin its population vector (PV) defined as the mean event rate of each cell given that bin's occupancy. This procedure was done separately for right and left running directions while considering only periods when the

Please cite this article in press as: Geva et al., Time and experience differentially affect distinct aspects of hippocampal representational drift, Neuron (2023), https://doi.org/10.1016/j.neuron.2023.05.005

mouse ran >2 cm/sec. Next, we excluded the last 2 bins at both ends of the tracks where water rewards were consumed and the mouse was generally stationary[3] and smoothed the activity of each cell across all spatial bins using a truncated Gaussian kernel (σ=1.5 bins, size=5 bins). Finally, we calculated the correlation between each population vector (PV correlation; see illustration in Figure 3A bottom right) in one session with that of the matching location in another session and averaged the correlations over all corresponding positions including only cells that were active (at least one Ca^{2+} event) in both sessions and significantly spatially tuned (i.e., place cells) in at least one of the two compared sessions. Specifically, in the analysis presented in Figure 2E, we calculated the PV correlation across all spatial locations, running directions, and environments while including all recorded cells across all sessions, as it has been shown that the same cells can exhibit different levels of spatial modulation when visiting different environments or under different running directions.[4] Furthermore, since in some cases the hippocampus can switch between multiple orthogonal maps (global remapping) across sessions in the same environment,[24] we separated between the different maps observed in each environment and considered for the within-environment analyses only PV correlations across sessions with the same map.

Ensemble rate correlation

To quantify the similarities in the population activity patterns between sessions, without accounting for changes in the tuning of individual cells, we calculated for each mouse the ensemble rate correlation between pairs of sessions that occurred in the same environment (see illustration in Figure 3A top right). First, we measured the Ca^{2+} event rate for each neuron in each session (irrespective of mouse position or running velocity) and then calculated the correlation between the activity rate vectors of neurons across all sessions. As with the PV correlation analyses, we restricted the analysis only to pairs of sessions with the same map.

Tuning curve correlation

To quantify the similarities in individual cells' tuning curves between sessions, without accounting for changes in their activity rates, we calculated for each mouse the tuning curve correlation between pairs of sessions that occurred in the same environment (see illustration in Figure 3A bottom left). After constructing the population vectors matrices as described above, we calculated the correlation between the tuning curve of each cell in one session with the tuning curve of the same cell in another session while considering only cells that were active (at least one Ca^{2+} event) in both sessions and significantly spatially tuned (i.e., place cells) in at least one of the two compared sessions. We used the mean correlation value across all cells to capture the central tendency of the entire population. As with the PV correlation analyses, we restricted the analysis only to pairs of sessions with the same map.

Relationship between activity rate and tuning curve stability (related to Figures S1L–S1O)

To examine the linear relationship between changes in individual cells' spatial tuning and firing rates, we calculated for each cell in a pair of consecutive sessions: (1) the tuning curve correlation, (2) mean activity rate, (3) absolute difference in activity rate, and (4) absolute difference in activity rate score between sessions (defined as the absolute difference in activity rate between the two sessions, divided by their sum). Then, we calculated for each mouse the coefficient of determination (R^2) to estimate the fraction of variation in the tuning curve correlations (changes in tuning) explained by either of these three quantifications of the neuronal activity rate including only cells that were active (at least one Ca^{2+} event) in both consecutive sessions and significantly spatially tuned (i.e., place cells) in at least one of the two compared sessions in the same environment.

Place fields characterization (related to Figures 4B–4F and S1E–S1G)

The position of the primary place field of each place cell was defined for each session and running direction separately as the spatial bin with the maximal Ca^{2+} event rate. In the analysis presented in Figure 4C, stable cells were defined as place cells that retained the location of their primary place-field between sessions ($\leq$4 cm shift).[53] To quantify the across-days stability of the primary place-field location (Figure 4D), we used the median absolute positional shift value across all neurons to capture the central tendency of the entire population. The number of place fields per place cell (Figures 4E, S1F, and S1G) was defined as the number of local maxima (using the *findpeaks* function with zero padding of the edges) with an activity rate that exceeds 33% of the event rate in the primary field after smoothing the activity of each cell across all spatial bins using a truncated Gaussian kernel (σ=1.5 bins, size=5 bins). The width of the primary place field (Figures 4F and S1E) was defined as the area around the center of the primary field position with an activity rate that exceeds 33% of the event rate in the primary field location without tuning curve smoothing.[53] To quantify the degree of stability of the number of place fields per place cell (Figure 4E) and the width of the primary place field (Figure 4F) across days, we used the mean absolute values across all neurons to capture the central tendency of the entire population. As with the PV correlation analyses, we restricted the analysis only to pairs of sessions with the same map.

Simulating representational drift (related to Figure S3)

To examine how changes in activity rates and changes in the tuning differentially impact representational drift as captured by the population vector correlation analysis, we simulated the neuronal activity of individual cells while parameterizing the degree of changes in their activity rates and tuning curves over time. We then ran the simulation under three different conditions: (1) Drift in both firing rates and tuning curves ("Full drift model" in Figure S3D left column); (2) Drift in tuning curves with stable activity rates ("Tuning drift model" in Figure S3D middle column); and (3) Drift in firing rates with stable tuning curves ("Rate drift model" in Figure S3D right column).

Please cite this article in press as: Geva et al., Time and experience differentially affect distinct aspects of hippocampal representational drift, Neuron (2023), https://doi.org/10.1016/j.neuron.2023.05.005

Specifically, to simulate the cells' activity rates, the activity rate of each cell on the first day of the simulation was randomly sampled from a log-normal distribution with $\mu = 0.0275$ Hz and $\sigma = 0.75$ Hz to resemble the mean firing statistics found in our dataset (as shown in Figure S1A). After each day, changes in the cells' activity rate were randomly sampled from a normal distribution ($\mu = 0$ Hz) and were added to the activity rate of the previous day. Cases in which the updated cells' activity reached below zero were rectified to zero. To better fit the ensemble rate correlation values to those found in our data, 75% of the total pool of neurons (N=1,000) were chosen randomly to be active on any given day.

To simulate the cells' tuning curves, each cell was randomly assigned a single preferred position on the first day of the simulation (out of 20 possible spatial bins along the linear track) from a uniform distribution, resulting in uniform coverage of place fields across the entire linear track. The activity pattern of each cell was then smoothed with a Gaussian kernel (σ=2 bins, size= 9 bins) and multiplied by its activity rate on that day. Based on our analyses in Figure 4, the changes in the cells' tuning curve in our simulation were restricted to positional shifts in the primary place field, and we did not allow changes in the number of fields or in the size of the primary place field. Specifically, after each day, changes in the cells' tuning curves were randomly assigned to 60% of the population and were normally distributed around zero positional shifts. To better resemble the tuning curve correlation values found in our data, 40% of the neurons were classified as place cells on any given day, while the rest of the cells were defined as non-place cells and were assigned a new, noisy tuning curve, in which the activity in each spatial bin was randomly sampled from a uniform distribution.

To gain insight into whether a putative downstream reader would be more affected by changes in the tuning or activity rates over time, we used the same simulation and trained a simple decoder (*k*-nearest neighbors, K=1, correlation distance) to infer the spatial location bin associated with a given population activity pattern on a given day (test data) based on the activity patterns of the neuronal population of a different day (training data). The performance of the decoder was defined as the percentage of correct classifications out of the 20 spatial bins for each pair of days.

Stability of occupancy and velocity profiles (related to Figures S4D and S4E)

To assess the consistency in mice behavior across sessions, we quantified for each mouse the similarity in its occupancy and velocity profiles between pairs of sessions that occurred in the same environment. We first divided the track into 24 spatial bins of equal size (4 cm each) and considered only periods when the mouse ran >2 cm/sec. The occupancy profile (Figure S4D) of each session was defined as the fraction of frames spent in each spatial bin regardless of the mouse's running direction. The velocity profile (Figure S4E) of each session was defined as the average velocity in each spatial bin and was calculated for each running direction separately. Then, we calculated the correlation between the occupancy profile or velocity profile vectors of each pair of sessions. Specifically, for the velocity profile analysis, we averaged the obtained correlation value over the two running directions to capture the velocity profile similarity across sessions.

Controlling for task performance variability (related to Figure S4F)

To control for the possibility that variability in the task performance of the mice (i.e., number of track traversals) across sessions or environments influenced our results, we randomly subsampled for each mouse the exact same number of track traversals for both running directions in all sessions of both environments. We then calculated for each mouse the ensemble rate, tuning curve, and population vector correlations between pairs of sessions (similar to Figures 3B–3D). The exact number of traversals sampled for all sessions was chosen for each mouse individually based on the session with the lowest number of traversals in either one of the two running directions. To obtain representative results across different traversal combinations, this procedure was repeated 1000 times for each mouse and then averaged across all realizations.

Relationship between neuronal code stability and behavioral variability (related to Figure S4G)

To quantitively assess the contribution of time, experience, and behavioral variability to driving representational drift, we calculated for each mouse the coefficient of determination (R^2). This allowed us to estimate the fraction of variation in the values of neuronal code stability quantifications (i.e., ensemble rate correlation, tuning curve correlation, and PV correlation) explained by either: (1) the elapsed time between visits; (2) the difference in the number of sessions between visits; (3) the absolute difference in the number of track traversals between visits; (4) the absolute difference in the average running speed between visits; (5) the similarity in the location occupancy between visits; and (6) the similarity in the velocity profile along the track between visits. The univariate linear model of each mouse was fit on pooled data of all pairs of sessions from both environments.

Statistical analysis

All statistical details, including the specific statistical tests, are specified in the corresponding figure legends. All analyses quantifying the differential effects of time and experience on the rate of representational drift were conducted at the level of individual mice. In general, for matched-pair samples, we performed a two-sided Wilcoxon signed rank test. In the cases of repeated-measurements of matched-pair samples, we used the Skillings–Mack test.[54] In all tests, significance was defined using α=0.05. We used the Pearson correlation coefficient to measure linear correlation. All statistical analyses were conducted using MATLAB 2017b (Mathworks).